Anal. Chem. **2005,** *77,* 3908−3915

Electrospray Diagnostics by Fourier Analysis of Current Oscillations and Fast Imaging

Lida Parvin, Marsha C. Galicia, Jennifer M. Gauntt, Leah M. Carney, Ann B. Nguyen, Eunyoung Park, Linda Heffernan, and Akos Vertes*

Department of Chemistry, Institute for Proteomics Technology and Applications, The George Washington University, Washington, D.C. 20052

The different spraying modes in electrospray ionization sources exhibit large variations in their ion yield and stability. To achieve consistently optimal ion production, active control of the spray parameters is desirable. To diagnose the changes in spraying mode, the spray current and its Fourier spectrum were monitored under a wide range of conditions, that is, as a function of the spray voltage, liquid flow rate, and composition. Most Fourier spectra indicated a strong dc component, a low-frequency branch at low flow rates and applied voltages, and a high-frequency branch and their harmonics. Changing of these parameters resulted in several spraying mode changes that were reflected in the Fourier spectra of the spray current. Significant mode changes and the malformation of the Taylor cone were detected as peak shifts or sudden changes in the spectrum quality. This was confirmed by fast imaging that showed a reduction in the size of the Taylor cone under hydrophobic tip conditions and rapid periodic ejection of filaments and droplets for high conductivity solutions. Comparing the oscillation frequencies of Taylor cones of different sizes, good correlation was found with the frequencies of capillary waves on comparablly sized liquid spheres. Spray stability was also linked with the positional stability of the contact line between the liquid meniscus and the capillary tip.

Two decades ago, electrostatic spraying was demonstrated to be a viable source of macromolecular ions.[1] Since then, this method of ion production has made a significant impact on the mass spectrometry (MS) of biomolecules.[2,3] By applying high voltage to a conducting liquid fed through a capillary, a variety of spraying modes, such as dripping, microdripping, spindle, Taylor cone, and multijet, can be induced.[4−7] Spray stability is impacted by capillary diameter (both inner and outer diameter), distance between the capillary and the counter electrode, capillary potential, liquid flow rate, and solution properties, that is, electrical conductivity, surface tension, viscosity, and dielectric constant.[6,8−11] The stability of the spray, in turn, is essential for the performance of the related analytical instruments. For example, electrospray ionization (ESI) is widely used as the interface between high performance liquid chromatography (HPLC) and MS. In the case of gradient elution, however, changes in the mobile phase composition during HPLC analysis may lead to spray instability and, subsequently, ion current variations in the mass spectrometer. Therefore, continuous monitoring of the spray and adjusting of its parameters seems desirable to maintain a stable and reliable ion current.[13] Recently, a method based on continuously monitoring the spray plume by a CCD camera and utilizing the obtained images in a feedback loop has been reported.[12]

The characterization of spraying modes through the observation of the dc mode current−voltage relationship between the capillary tip and the counter electrode yielded three different regions.[14,15] For acidified methanol solutions, the area at low voltages exhibited rapidly increasing currents corresponding to a pulsating Taylor cone. In a narrow range of intermediate voltages, a cone jet was generated, and the current stayed almost constant. In the third region, at higher voltages, the current rapidly increased, indicating a multijet spray.

On the basis of dimensional analysis, for systems in cone-jet mode, an empirical expression was described for the dc spray current, I_{dc}, as[9]

$$I_{dc} \sim \left(\frac{\gamma Q K}{\epsilon_r}\right)^{1/2} \quad (1)$$

where Q is the volumetric liquid flow rate, K is the electrical conductivity, and γ and ϵ_r are the surface tension and the relative permittivity of the liquid, respectively. In a follow-up study for

* Corresponding author. Phone: (202) 994-2717. Fax: (202) 994-5873. E-mail: vertes@gwu.edu.

(1) Yamashita, M.; Fenn, J. B. *J. Phys. Chem.* **1984**, *88*, 4451−4459.
(2) Cole, R. B. *Electrospray Ionization Mass Spectrometry: Fundamentals, Instrumentation, and Applications*; Wiley: New York, 1997.
(3) Griffiths, W. J.; Jonsson, A. P.; Liu, S.; Rai, D. P.; Wang, Y. *Biochem. J.* **2001**, *355*, 545−561.
(4) Zeleny, J. *Phys. Rev.* **1917**, *10*, 1−6.
(5) Cloupeau, M.; Prunet-Foch, B. *J. Electrost.* **1989**, *22*, 135−159.
(6) Grace, J. M.; Marijnissen, J. C. M. *J. Aerosol Sci.* **1994**, *25*, 1005−1019.
(7) Jaworek, A.; Krupa, A. *J. Aerosol Sci.***1999**, *30*, 873−893.
(8) Cloupeau, M.; Prunet-Foch, B. *J. Aerosol Sci.* **1994**, *25*, 1021−1036.
(9) Fernandez de La Mora, J.; Loscertales, I. G. *J. Fluid Mech.* **1994**, *260*, 155−184.
(10) Wilm, M.; Mann, M. *Anal. Chem.* **1996**, *68*, 1−8.
(11) Noymer, P. D.; Garel, M. *J. Aerosol Sci.* **2000**, *31*, 1165−1172.
(12) Valaskovic, G. A.; Murphy, J. P., III; Lee, M. S. *J. Am. Soc. Mass Spectrom.* **2004**, *15*, 1202−1215.
(13) Charbonnier, F.; Rolando, C.; Saru, F.; Hapiot, P.; Pinson, J. *Rapid Commun. Mass Spectrom.* **1993**, *7*, 707−710.
(14) Jackson, G. S.; Enke, C. G. *Anal. Chem.* **1999**, *71*, 3777−3784.
(15) Cech, N. B.; Enke, C. G. *Mass Spectrom. Rev.* **2001**, *20*, 362−387.

10.1021/ac050475e CCC: $30.25
Published on Web 05/10/2005

liquids with low viscosity and conductivity, a different relationship was found,[24]

$$I_{dc} \sim (\gamma^3 \epsilon_0 QK/\rho)^{1/4} \quad (2)$$

where ρ is the liquid density and ϵ_0 is the vacuum permittivity. It is important to recognize that for liquids of significance in ESI, stable cone-jet mode is rarely achieved. It was even argued that for certain solutions (e.g., acidified 10% methanol) it cannot be established.[15]

On the basis of measuring the ac component of the current in methanol solutions, Juraschek and Röllgen established a different classification of spraying modes, that is, axial modes I, II, and III and nonaxial or rim emission modes.[16] Their cone imaging data assigned axial modes I and II as pulsating cone jets and axial mode III as the stable cone jet. Axial mode I existed at lower voltage values, for example, 2.1 kV, and was characterized by both low- and high-frequency current pulsations at, for example, ~30 Hz and 1−2 kHz, respectively. By increasing the voltage (in the 2.2−3.1-kV range), axial mode II was observed that exhibited only the high-frequency current oscillations. Juraschek and Röllgen hypothesized that the imbalance between liquid loss through emission and the liquid supply through the capillary created the current pulsations.[16] Further increasing the voltage resulted in a transition of the spraying mode to axial mode III, where continuous emission of droplets occurred from a stable cone jet and a constant current was measured. Axial modes I and II involved the process of Taylor cone pulsation, ejection of a liquid jet, and its break up into charged droplets. Using Fourier analysis of the spray current[25] and fast imaging, evidence of a direct relationship between the mechanical pulsations of the Taylor cone and the spray current oscillations was reported.[17]

Droplet size and velocity changes in the spray plume of ESI sources were studied using phase Doppler anemometry (PDA).[18,19] The conductivity of the sprayed liquid and the dimensions of the spraying capillary had a profound effect on the droplet diameter distributions. Ion formation from charged nanodroplets was followed using molecular dynamics simulations.[20] Ejection of solvated ions was observed from these nanodroplets through the detachment of extreme protrusions.

Formation of primary droplets close to the end of the spraying capillary was studied by fast imaging methods.[21] To capture the ejection of charged liquid, short exposure time (0.5 μs) and high frame rate (67 kHz) were essential. These studies provided insight on a great diversity of jet disintegration modes, including varicose, ramified, and kink jet breakup into primary droplets. As a consequence of solvent loss due to evaporation, these droplets approach the Rayleigh limit and fission. This process was studied using flash shadowgraphy[22] and PDA.[18,19]

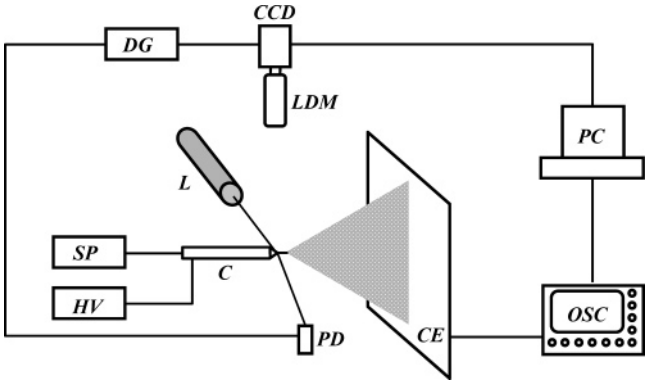

Figure 1. Schematic diagram of experimental setup. Liquid was pumped by a syringe pump (SP) through a blunt tip metal capillary (C) held at high voltage by a stabilized power supply (HV). Time dependence of spray current on counter electrode (CE) was measured by an oscilloscope (OSC) and transferred to a computer (PC). Images were taken through a long-distance microscope (LDM) using either a regular or a fast CCD camera (CCD). When needed, triggering signal was provided through a digital delay generator (DG) by a photodiode (PD) that responded to a He/Ne laser beam (L) refracted by the protruding liquid meniscus.

In this paper, we report on the analysis of both the dc and the ac components of the spray current as diagnostic tools for spraying mode changes. To determine characteristic oscillation frequencies, we monitored and analyzed the Fourier spectrum of the spray current at various spray voltages and liquid flow rates. Furthermore, we investigated the effect of liquid composition on the Fourier spectrum of the current signal. Using fast imaging, we correlated changes in the Fourier components with specific jet and droplet ejection modes. Malformation of the Taylor cone due to incomplete wetting of the capillary tip was also detected as a significant change in the Fourier spectrum. The objective of this effort was to establish a diagnostic tool for spray stability under conditions of changing liquid properties and to help select the proper spraying parameters for ESI analysis.

EXPERIMENTAL SECTION

Figure 1 shows the schematics of the experimental setup for current measurements and fast imaging. A home-built electrospray system with a syringe pump (model 22, Harvard Apparatus, Holliston, MA) was used to spray methanol−water and acetonitrile−water mixtures of various compositions through a blunt tip stainless steel capillary (model 90531, i.d. = 130 μm, o.d. = 260 μm, Hamilton Co., Reno, NV). The capillary was accurately positioned in the *x*, *y*, and *z* directions using mechanical translation stages (F38182 and NT37-979, Edmund Industrial Optics, Barrington, NJ). Stable potential to generate the electrospray was provided by a regulated high voltage power supply (model PS350, Stanford Research Systems, Inc., Sunnyvale, CA). A flat, stainless steel counter electrode was positioned perpendicular to the capillary at 30.0 mm from its tip. The capillary current was measured by a digital oscilloscope (LC9370M, LeCroy, Chestnut Ridge, NY) through its 1-MΩ input using dc coupling with a

(16) Juraschek, R.; Röllgen, F. W. Int. *J. Mass Spectrom.* **1998**, *177*, 1−15.
(17) Marginean, I.; Parvin, L.; Heffernan, L.; Vertes, A. *Anal. Chem.* **2004**, *76*, 4202−4207.
(18) Olumee, Z.; Callahan, J. H.; Vertes, A. *J. Phys. Chem. A* **1998**, *102*, 9154−9160.
(19) Olumee, Z.; Callahan, J. H.; Vertes, A. *Anal. Chem.* **1999**, *71*, 4111−4113.
(20) Znamenskiy, V.; Marginean, I.; Vertes, A. *J. Phys. Chem. A* **2003**, *107*, 7406−7412.
(21) Hartman, R. P. A.; Brunner, D. J.; Camelot, D. M. A.; Marijnissen, J. C. M.; Scarlett, B. *J. Aerosol Sci.* **2000**, *31*, 65−95.
(22) Gomez, A.; Tang, K. *Phys. Fluids* **1994**, *6*, 404−414.
(23) Landau, L. D.; Lifshitz, E. M. *Fluid Mechanics*, 2nd ed.; Butterworth Heinemann: Woburn, MA, 2003; p 247.
(24) Ganan-Calvo, A. M.; Davila, J.; Barrero, A. *J. Aerosol Sci.* **1997**, *28*, 249−275.
(25) Gauntt, J. M.; Vertes, A. *Proc. 48th ASMS Conf. Mass Spectrom. Allied Top.* **2000**, 212−213.

bandwidth limit of 25 MHz. A CCD camera (model GP-KR222, Panasonic, Secaucus, NJ) and a long-distance microscope with primary magnification of 0.9−1.3× (IF3, Edmund Scientific, Barringer, NJ) were used for continuous visualization of the spray that was illuminated with a light source through fiber optics (model 150 Illuminator, RAM Optical Instrumentation, Inc., Irvine, CA). Surrounding the system by a plexiglass enclosure minimized disturbances from ambient airflow.

In principle, there are two options to follow the spray current. It can be determined either at the spraying capillary or at the counter electrode. There are obvious benefits and drawbacks to both. While the current at the capillary is a more direct measure of the emitted charge, it is less relevant in terms of the working of an ESI source. Typically, the sampling cone in the atmospheric pressure interface of the mass spectrometer acts as the counter electrode. The current measured on it is more indicative of the stream of charged droplets entering the reduced pressure region in the interface. Therefore, we decided to measure the current on the counter electrode.

Because the typical current readings were in the low nanoampere range, special care was taken to provide adequate electrical shielding and grounding. First, the environmental noise spectrum was recorded with no spray running; i.e., the entire system was turned on, but the pump was set to zero flow rate. Obvious electrical noise sources were identified (power cords, light fixtures, monitors, etc.) and shielded or eliminated, leaving the background practically interference-free in the 0−10 kHz region of interest.

Slight differences in the spray were observed when the desired voltage was established through either decreasing or increasing the potential to the desired value. Because of this hysteresis effect and a slight drift in the current signal following adjustments, the flow rate and the applied voltage were varied systematically, and data collection was carried out after a 10-min waiting period at every new setting.

For each measurement, 100 000 data points were acquired by the oscilloscope at minimum 20 kHz sampling rate and transferred to a personal computer through the GPIB interface utilizing LabVIEW (ver.6i, National Instruments, Austin, TX) software. Fourier analysis of the current waveforms was performed with a scientific visualization package (Origin 6.0, OriginLab Co., Northampton, MA). In compliance with the dataset size requirementfor the fast Fourier transform algorithm, 65 536 (2^{16}) data points were utilized. The chosen length of observation resulted in the best peak shapes in the Fourier spectra, while the selected sampling rate satisfied the Nyquist criterion for the frequency domain of interest.

Images of the Taylor Cone. For fast imaging studies, the regular CCD camera described earlier was replaced by a fast imaging device (QICAM, QImaging, Burnaby, BC) with 40-μs exposure time. For periodic meniscus deformations, triggering for this camera was provided by a fast photodiode (model Det210, Thorlabs, Newton, NJ) that detected the light of a 0.5-mW HeNe laser (model 05-LLR-811, Melles Griot, Carlsbad, CA) deflected by the meniscus at the end of the spraying capillary. A digital delay generator (model DG535, Stanford Research Systems, Sunnyvale, CA) enabled the introduction of a controlled time difference between the trigger signal and the camera exposure.

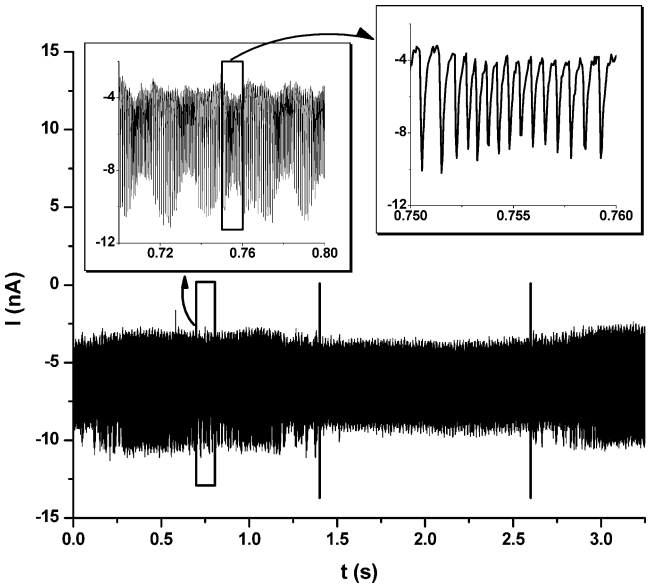

Figure 2. Time dependence of spray current for 50% MeOH at 0.5 μL/min and 2.9 kV shows nested high and low-frequency oscillations (see zoomed regions in the insets) with periodic (in the 1.4 s < t < 2.6 s region) and quasiperiodic (in the t < 1.4 s and t > 2.6 s domains) low-frequency behavior. Outside the region of stability, the low-frequency oscillations change from quasiperiodic to aperiodic. Nonlinearities in the current oscillations, discernible from the shape of the $I(t)$ curve in the second inset, give rise to generation of harmonics in the Fourier spectra.

Materials. HPLC grade methanol (MeOH) and acetonitrile (ACN) were purchased from Aldrich and Fischer, respectively. The solutions were prepared with deionized water (18.3 MΩ/cm, produced by a D4631 E-pure system, Barnstead, Dubuque, IA). Higher conductivity solutions were prepared using 0.1% trifluoroacetic acid (TFA) (reagent grade from Aldrich). The electrical conductivity of the solutions was measured by a conductivity meter (YSI 3100, YSI Inc., Yellow Springs, OH) with a dip cell utilizing a built-in thermistor (YSI 3256, YSI Inc., Yellow Springs, OH). Temperature-compensated conductivities at 25 °C for these solutions were 1.40 μS for 50% MeOH, 0.61 μS for 50% ACN, and 72.7 μS for 90% MeOH prepared in 0.1% TFA. The sprayed solutions were freshly prepared before each set of experiments.

RESULTS AND DISCUSSION

In all experiments, the spray current as a function of time, $I(t)$, showed remarkable complexity. Typically, the current exhibited a strong dc component, I_{dc}, and periodic, quasiperiodic, or aperiodic oscillations, which often included nested oscillations. The quasiperiodic and aperiodic behavior was observed at higher voltages or at low flow rates. For example, the time-dependence of the spray current, $I(t)$, for 50% MeOH at 0.5 μL/min and 2.9 kV in Figure 2 shows nested high- and low-frequency oscillations (see zoomed regions in the insets) with periodic (in the 1.4 s < t < 2.6 s region) and quasiperiodic (in the t < 1.4 s and t > 2.6 s domains) low-frequency behavior. The dc component of the current can also be observed in Figure 2 as a negative offset. The first inset on the left shows the low-frequency oscillations as the envelope of the high-frequency oscillations. Outside the region of stability for the spray parameters, these low-frequency oscilla-

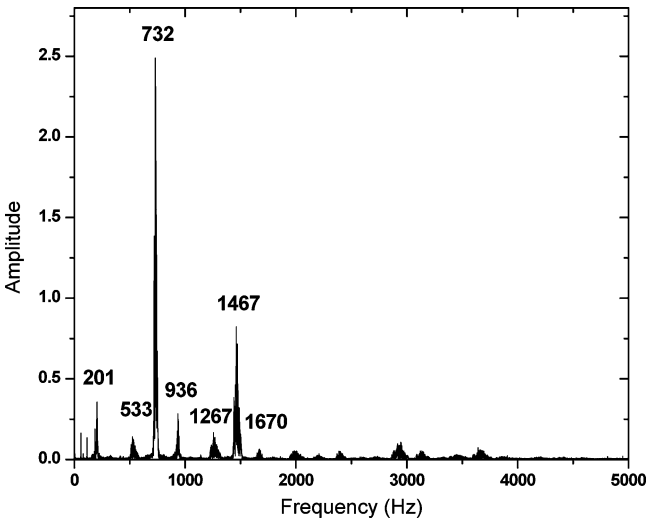

Figure 3. Fourier amplitude spectrum of spray current for 50% ACN in water sprayed at 2.0 μL/min flow rate and a spray voltage of 2.5 kV. Oscillations at low frequency, f_{low} = 201 Hz; high frequency, f_{high} = 762 Hz; its second harmonic, 2 × f_{high} = 1467 Hz; and their combinations with the low-frequency mode, $f_{high} \pm f_{low}$ = (533, 936 Hz) and 2 × $f_{high} \pm f_{low}$ = (1267, 1670 Hz) are observed.

tions change from quasiperiodic to aperiodic or disappear completely. The second inset on the right shows the fine structure of high-frequency pulsation. These current oscillations are more robust than their low-frequency counterparts and can be observed under most studied conditions.

Current data was collected for a wide range of spray parameters: the spray voltage was changed between 2.3 and 5.0 kV, and the liquid flow rate was selected between 0.5 and 16.0 μL/min. Three different solutions were sprayed: 50% MeOH; 50% ACN; and to probe a high conductivity case, 90% MeOH prepared in 0.1% TFA. Depending on the spray parameters, primarily voltage, flow rate, and geometry, and on the physical properties of the sprayed liquid, most importantly, the electrical conductivity, the different components of the current became more or less dominant. For the purposes of ion production, quasiperiodic and aperiodic oscillations are considered to be instabilities; thus, we have focused our attention on exploring the periodic behavior.

Fourier transformation of the spray current was used to analyze its periodic features. Figure 3 shows a typical Fourier amplitude spectrum of the spray current for 50% ACN solution sprayed at 2.0 μL/min flow rate and 2.5-kV capillary voltage. Due to its much larger amplitude, the dc component at zero frequency was eliminated and plotted separately (see later). Similar spectra were obtained for various spraying conditions and other liquids (50% and 90% MeOH prepared in 0.1% TFA). In general, the Fourier spectra exhibited a low-frequency branch (<500 Hz, most pronounced at low flow rates and applied voltages); a high-frequency branch (0.5−7 kHz); their harmonics; and occasionally, their combination frequencies. In Figure 3, one can observe the oscillations at low frequency, f_{low} = 201 Hz; at high frequency, f_{high} = 732 Hz; at its second harmonic, 2 × f_{high} = 1467 Hz; and at their combinations with the low-frequency mode, $f_{high} \pm f_{low}$ = (533, 936 Hz) and 2 × $f_{high} \pm f_{low}$ = (1267, 1670 Hz). As it is demonstrated below, the exact position and intensity of these components vary with changing operating parameters, such as the liquid flow rate, the capillary voltage, the capillary diameter, and the physical properties of the sprayed solution.

It was shown in a previous publication that in simple Fourier spectra with only the high frequency branch present, the principal frequency of current oscillations is directly linked to the frequency of Taylor cone pulsations.[17] On the basis of this simple correlation, one might expect to be able to find separate electrohydrodynamic processes responsible for the low frequency branch, the harmonics, and the combination frequencies. Indeed, on the basis of fast imaging observations, the low-frequency branch can be connected with a slow swelling of the Taylor cone and the occasional ejection of the excess material. There was no indication, however, of a separate physical process responsible for the harmonics and the combination frequencies. Instead, nonlinearities in the Taylor cone oscillation can be invoked to account for the emergence of these higher order components in the Fourier spectrum. Conversely, the emergence of aperiodic behavior at high voltages does have a physical origin; namely, it can be associated with the chaotic dynamics of Taylor cone deformations.

The effect of the spray voltage on the principal frequencies was investigated by systematically changing its value between 2.2 and 3.8 kV. In Figure 4a, the two vertical lines separate axial modes I and II and the rim emission mode observed for the low conductivity solvents 50% MeOH (solid line) and 50% ACN (dotted line). At low voltages, axial mode I prevailed, with both a low- and a high-frequency branch present. Increasing the voltage beyond 2.5 kV, axial mode II set resulted in the loss of the low frequency branch and more robust high frequency oscillations. In this region, the principal frequencies gradually climbed with increasing voltage. At 3.1 kV, the spray directly transitioned into rim emission mode (without entering axial mode III), and the stability decreased. Depending on the rate of establishing the voltage, for 50% MeOH, a metastable branch was also observed (dashed line). Fast imaging (see insets in Figure 4a) revealed that the stable and metastable rim emission branches differ in the geometry of the meniscus. The lower frequency metastable mode corresponded to single jet emission, whereas the higher frequency stable mode showed dual jet emission. The position of jet emission did not seem stationary, but varied in time. This indicated the formation of complex capillary wave patterns on the surface of the meniscus. Further increasing the voltage resulted in the loss of periodic oscillations and the onset of chaotic behavior. Although current pulsations were clearly present, due to the lack of periodicity, the Fourier spectra did not show well-defined peaks and only occasionally exhibited some very broad features.

Figure 4b shows the current oscillation frequencies for 50% MeOH and 50% ACN solutions sprayed at different flow rates with the capillary voltage held at 2.9 kV. Below 1.0 μL/min in axial mode I, the sprays were unstable, and the Fourier spectra of the current were noisy with some broad features present (left inset panel). These attributes of the Fourier spectra indicated the presence of substantial aperiodic oscillations. For 50% MeOH, however, well-defined, low-frequency oscillations were also recognized. In general, aperiodic fluctuations tended to emerge from low-frequency oscillations; thus, they first obscured the peaks in the low-frequency branch. For both solutions, increasing the flow rate in the 1.0−4.0 μL/min range slightly increased the principal

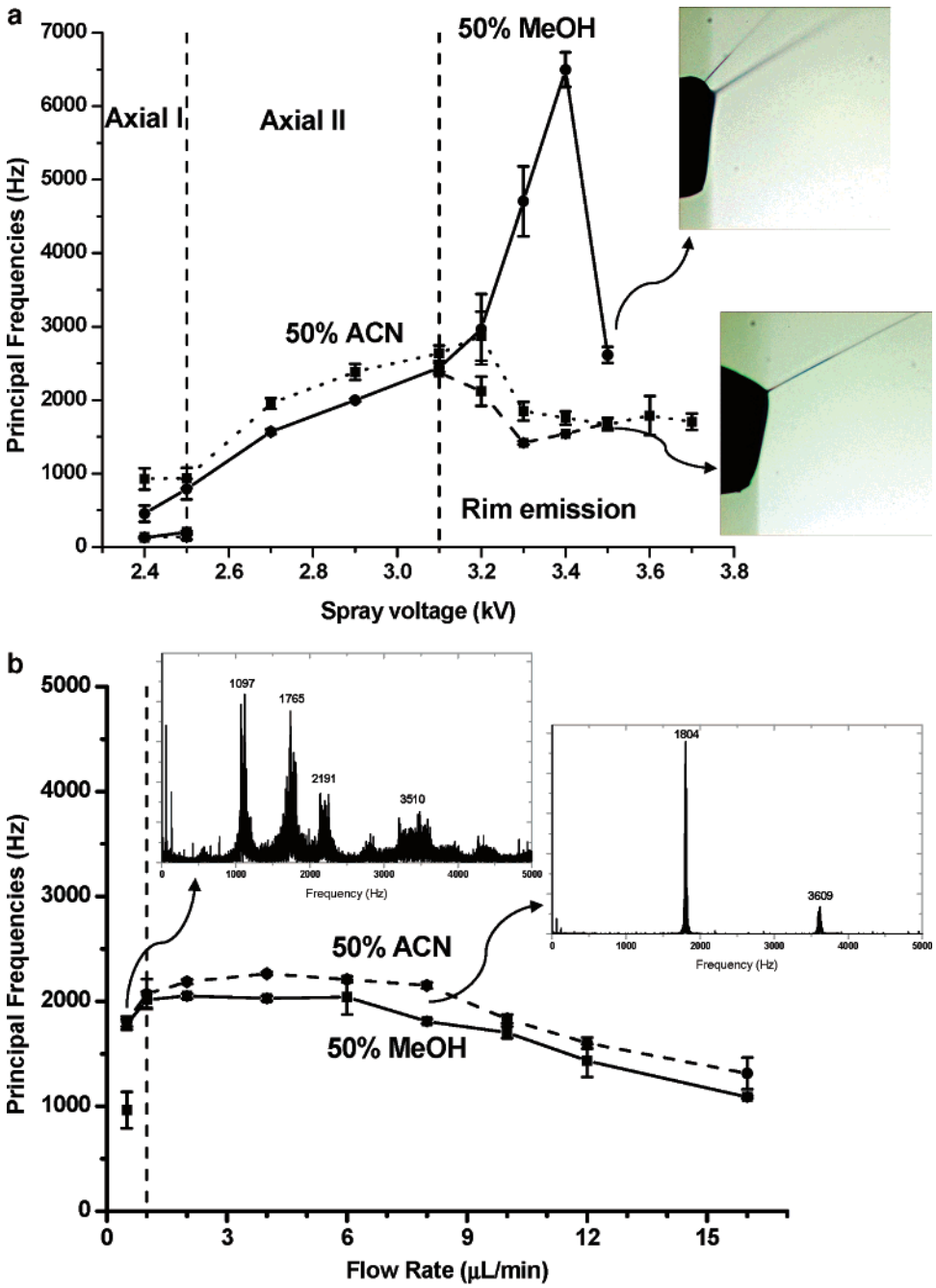

Figure 4. Principal frequencies from Fourier amplitude spectra of spray current for 50% MeOH (■) and 50% ACN (●) solutions (a) as a function of applied voltage sprayed at 2.0 μL/min flow rate and (b) as a function of liquid flow rate sprayed at 2.9 kV. In part a, the insets show fast images of the menisci corresponding to the stable (solid) and metastable (dashed) regime in rim emission mode. In part b, the left and right inset panels show the Fourier spectra of the 50% MeOH solution sprayed at 0.5 μL/min and 8.0 μL/min, respectively.

frequencies. Further increase in the 4.0−16.0 μL/min range resulted in a slow decline in the principal frequencies. At intermediate flow rates, a cleaner background and well-defined peaks in the spectra (right inset panel) indicated improved spray stability.

Interestingly, the dc component of the spray current in axial mode II followed Ohmic behavior. In Figure 5a, this is confirmed for 50% MeOH by a linear fit to this section of the curve. Linear regression of the empirical relationship yielded $I_{dc} = a + bU_{sp}$ where $a = 2.7$ nA and $b = 3.4 \times 10^{-12}$ Ω^{-1} with a regression coefficient of $R = 0.996$. This corresponds to the behavior of a poor insulator with a resistance of ~300 GΩ. The amplitude of the ac component in this region was essentially constant at ~10% of the dc component.

As the spray voltage was further increased, the spray entered the rim emission mode. Both the dc and the amplitude of the ac component initially decreased with increasing voltage. This behavior cannot be attributed to a passive electronic component because it corresponds to negative resistance. A possible explanation for this behavior is the change in the spray geometry when the system crosses over from axial mode II to rim emission mode. Because spray current is measured on the counter electrode, it is prone to artifacts resulting from incomplete collection of the charged droplets. Thus, when the spray switches from the forward

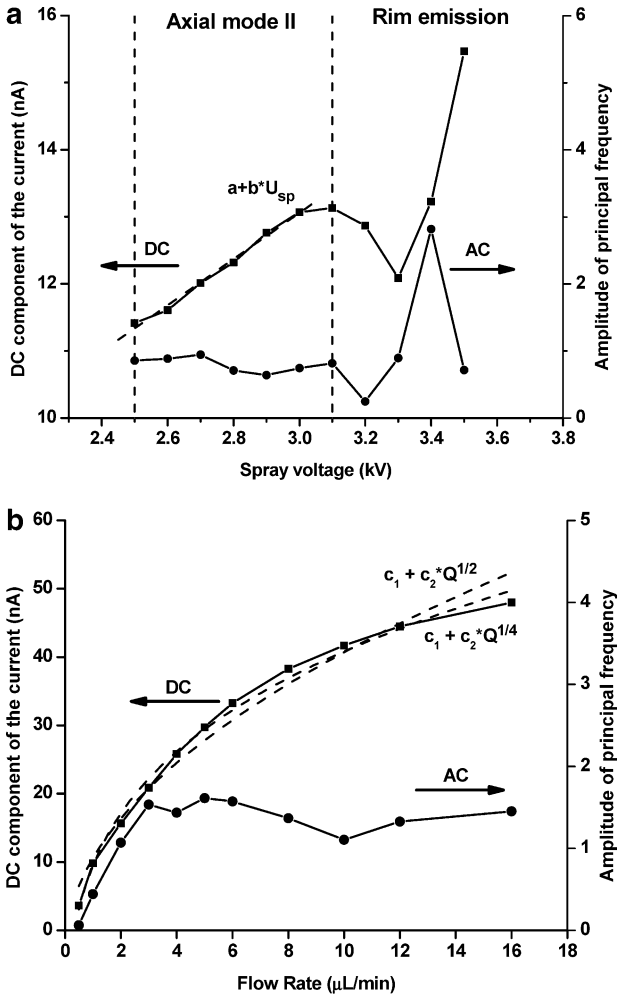

Figure 5. Direct current component and amplitude of the principal frequency of the spray current as a function of (a) spray voltage for 50% aqueous MeOH solution sprayed at 2.0 μL/min and (b) liquid flow rate for the same solution sprayed at 2.9 kV. In part a, the linear fit shows the Ohmic contribution, whereas in part b, the two fitted lines compare the empirical models behind eqs 1 and 2 with our experimental data.

directed plume in axial emission to more broadly distributed plume in rim emission, some of the charged droplets may not make it to the counter electrode. This is registered as a drop of current if the amount of lost charge is proportional to the applied voltage; i.e., the plume opens up with increasing voltage. Further increase of the spray voltage resulted in a sharp increase of both I_{dc} and the amplitude of I_{ac}. The fast increasing spray current in this region can be an indication that the growing amount of charge carried by the droplets and perhaps the improved collection efficiency at higher fields overcome the loss of charge due to the change in plume geometry. The final drop in the amplitude of the ac component at 3.5 kV could be understood considering the onset of chaotic emission and, consequently, the loss of periodicity in the spray current.

Throughout the entire studied region, the dc component of the current grew monotonically with increasing flow rate of the sprayed solution (Figure 5b). To characterize the functional relationship between I_{dc} and the flow rate, Q, we fitted the data points in Figure 5b with the power law relationships based on eqs 1 and 2: $I_{dc} = c_1 + c_2Q^{\beta}$ where $\beta = 1/2$ for eq 1 and $\beta = 1/4$ for eq 2. Both functions gave acceptable fits, with clearly better regression coefficients for the $\beta = 1/4$ case: $R_{\beta=1/4} = 0.997$ compared to $R_{\beta=1/2} = 0.989$. These results present a valuable extension of eqs 1 and 2, originally derived only for cone jet mode, that is, axial mode III.[9,24] In our experiments, varying the flow rate from 0.5 to 16.0 μL/min, the spraying mode changed from axial mode I through axial mode II to rim emission mode without encountering axial mode III at all. Nevertheless, the equations developed to describe the $I_{dc} = f(Q)$ relationship in the steady-state axial mode III seem to be valid throughout the various pulsating modes. After rapid initial growth, the ac component of the current, plateaued at 3.0 μL/min and remained essentially constant at higher flow rates. Comparing Figures 4b and 5b in this region indicates steady ac amplitudes with slightly declining frequency. Thus, the increasing current is primarily carried away by the dc component.

Outside the chaotic regime, the relative importance of the dc and ac current components can be also discerned from Figure 5. The ratio of the ac amplitude to the dc current, I_{dc}, changes with changing spray parameters. From the data in Figure 5a, the contribution of the ac amplitude is determined to be between 2 and 21%, depending on the spray voltage. The flow rate dependence of the ac current contribution varies between 2 and 7%. On the basis of the mechanism of oscillation identified in ref 17, one expects this contribution to increase when the counter electrode is moved closer to the spraying capillary. This is expected because the charged liquid is emitted intermittently in finite jets from the Taylor cone. At that stage, the current is purely alternating; i.e., there is no dc component. Downstream from the capillary, as the jet disintegrates into droplets, the initially discrete packets intermingle, thereby introducing an apparent dc component.

In addition to the discussed spray parameters, the geometry and physical properties of the capillary play an important role in the current oscillations. Figure 6 shows the images of wetted and nonwetted capillary tips in Figure 6a and b, respectively, and the corresponding Fourier spectra of the spray current (Figure 6c and d). Figure 6a shows the pulsating Taylor cone seated on the entire cross section of the capillary tip with the contact line of the meniscus pinned to the outer edge of the tip. When the sprayed liquid readily wets the capillary surface, this is the regular form of the Taylor cone. If wetting is inhibited on the front surface, the contact line of the meniscus is anchored to the inner edge of the tip. This results in a malformed Taylor cone that contains a much smaller volume of the sprayed liquid (Figure 6b). Fourier analysis of the spray current for regular and malformed Taylor cones indicates that for the latter, spray oscillations shift to dramatically higher frequencies (compare Figure 6c and d). Spraying 50% MeOH solution at 2.0 μL/min and 2.9 kV resulted in a Taylor cone that oscillated at $f_0 = 2.0$ kHz when fully formed (the peak at 4.0 kHz is the second harmonic) but at $f_0 = 4.4$ kHz in the malformed case.

Among all the factors we have studied, the position of the contact line and, correspondingly, the size of the Taylor cone have the most significant impact on the frequency of current oscillations. This implies that unnoticeable changes in the position of the contact line may result in sizable frequency changes and, as a consequence, undermine spray stability. Thus, the wetting properties and the geometry of the capillary tip emerge as

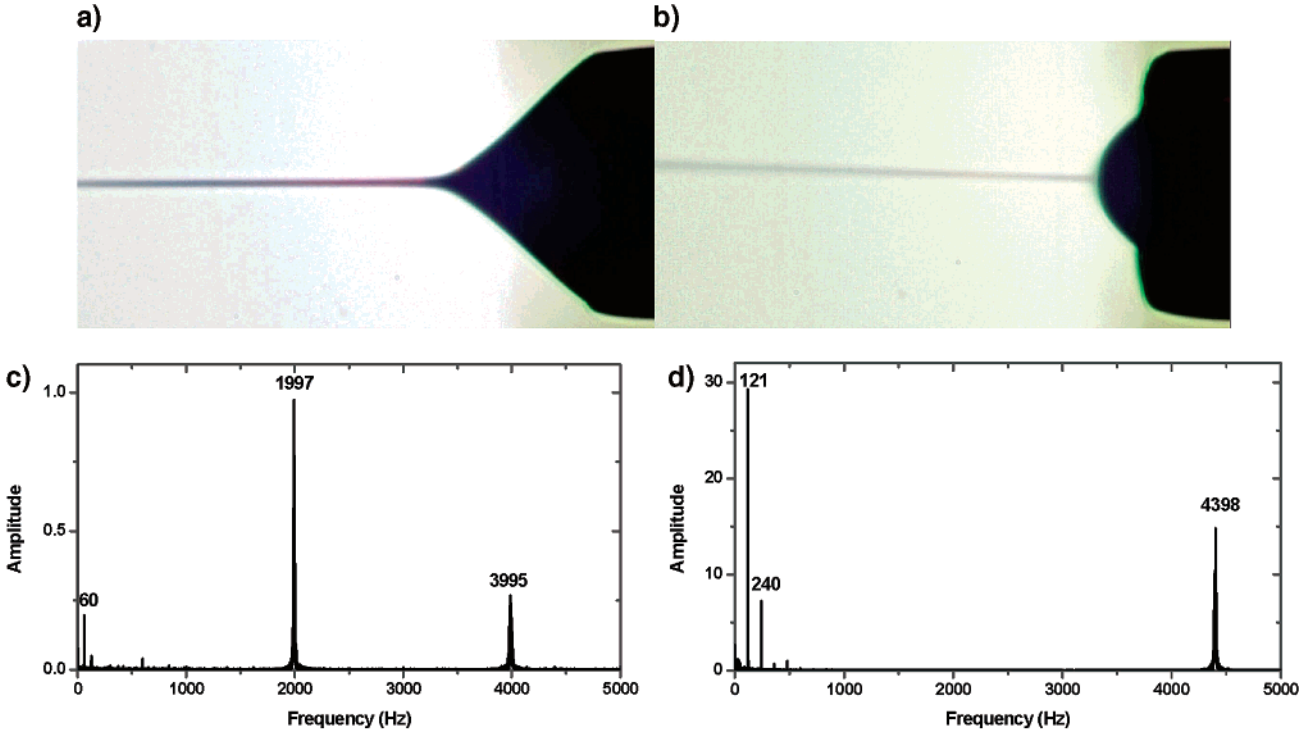

Figure 6. Images of Taylor cone on wetted (a) and nonwetted (b) capillary tip and the corresponding Fourier amplitude spectra of the spray current, (c) and (d), respectively, for 50% MeOH solution at 2.0 μL/min flow rate and 2.9-kV spray voltage. Malformation of the Taylor cone (part b) is reflected in dramatic shift in the principal frequency of current oscillations.

paramount factors in producing stable sprays. Furthermore, after changing the flow rate or the spray voltage, slow movement of the contact line on the tip surface may occur which could explain the drift and hysteresis effects mentioned in the Experimental Section.

There is a remarkable correlation between the reduced volume of the malformed Taylor cone (Figure 6b) and the shift in the principal frequency to higher values (Figure 6d). This behavior resembles the natural oscillations of a spherical drop due to capillary waves. The oscillation frequency for the lowest excitation mode, f_0, of a liquid sphere can be written as[23]

$$f_0 = \frac{1}{2\pi}\left(\frac{8\gamma}{\rho R^3}\right)^{1/2} \tag{3}$$

where R is the radius. In qualitative agreement with our observations, decreasing the radius of the protruding liquid sphere at the end of the capillary, that is, the Taylor cone, results in higher oscillation frequency. This correlation indicates that the bulk of our observations in Figure 6 can be explained by pure volume effects.

One can argue that under axial spraying conditions, this spherical approximation is realistic. Looking at the images of the oscillating Taylor cone in ref 17, it is clear that the oscillating liquid protruding from the capillary has a hemispherical shape, especially during phases I and IV (see Figure 1 in ref 17). Using eq 3 and $\gamma = 35.6$ mN/m and $\rho = 0.92$ g/cm^3 for 50% MeOH, the calculated frequencies are $f_0(R = 130\ \mu\text{m}) = 1.9$ kHz in the case of a Taylor cone based on the o.d. of the capillary and $f_0(R = 65\ \mu\text{m}) = 5.3$ kHz in the case of the malformed Taylor cone based on the capillary i.d. The measured principal frequency values in Figure 6c and d are $f_0(R = 130\ \mu\text{m}) = 2.0$ kHz and $f_0(R = 65\ \mu\text{m}) = 4.4$ kHz. For the 15-μm-i.d. capillary in ref 12, eq 3 yields a significantly higher frequency, $f_0(R = 7.5\ \mu\text{m}) = 136$ kHz. The reported values for the oscillation frequency in cone-jet mode in that publication were 102 kHz at 250 nL/min. This comparison indicates a reasonable agreement of measured and calculated oscillation frequencies for such a simple mechanical model. Clearly, a more involved analysis is needed to express the influence of the electrified surface on the capillary wave frequencies.

The effect of increased conductivity on the spray current and meniscus geometry was studied using 90% MeOH prepared with 0.1% TFA. This system exhibited an electrical conductivity of 73 μS, as compared to the ~1 μS conductivity of the other two systems. An increase of almost 2 orders of magnitude in conductivity had a profound effect on the sprays. Whereas the Fourier spectra of current oscillations showed increased stability in the principal frequencies, the amplitude of oscillations steadily declined with increasing voltage (see Figure 7). Figure 7a shows a Fourier spectrum at 2.9 kV spray voltage with a principal frequency of 1235 Hz and a rich variety of harmonics. At 3.9 kV, the peak amplitudes are reduced (Figure 7b), and the higher harmonics disappear. There are some broad features in the background, indicating the presence of occasional ill-defined frequency shifts in the current pulsation. The 617-Hz peak barely visible at 2.9 kV becomes stronger, along with its harmonics. At 5.0 kV, the trend continues. A low frequency oscillation appears at 27 Hz, and the 618 Hz peak becomes the principal frequency, with two of its harmonics present. Combination frequencies of the 27-Hz oscillation and the high-frequency peaks appear in the spectrum. The amplitudes are further diminished to ~1/10 of the

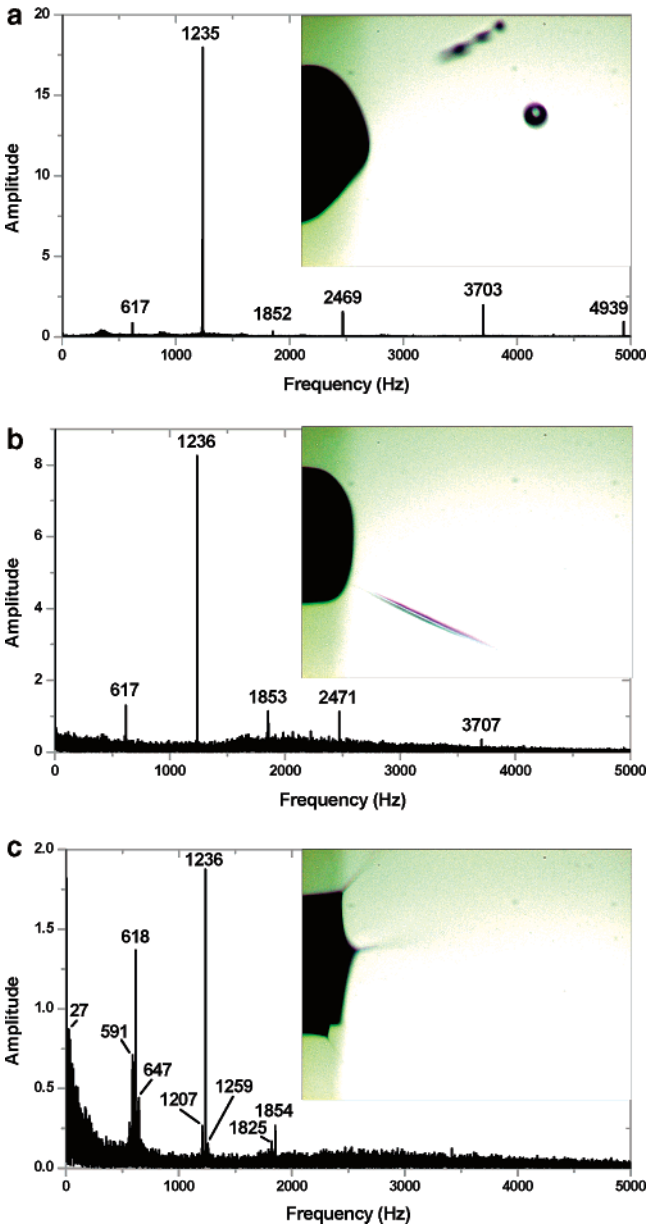

Figure 7. Increased conductivity changes the spraying modes and their onset voltages. Dependence of Fourier spectra on spraying mode for 90% MeOH solution prepared in 0.1% TFA is demonstrated for 4.0 μL/min flow rate and spray voltages of (a) 2.9, (b) 3.9, and (c) 5.0 kV. Corresponding fast images of the meniscus show rapid ejection of droplets, filaments, and jets at the rim, respectively.

values observed at 2.9 kV. A broad tail of the low-frequency peak indicates great uncertainties in this frequency.

Fast imaging of the corresponding menisci revealed that the spraying modes introduced for low-conductivity systems need to be revised. Instead of the succession of axial modes I, II, and III, already at low voltages, the liquid is rapidly ejected at an oblique angle. In the inset of Figure 7a, the image of the meniscus at 2.9 kV reveals the ejection of a droplet along with the departure of a filament that breaks up into three droplets. At 3.9 kV, the image in the inset of Figure 7b shows a thin filament emitted. Even though this system is not in rim emission geometry, the departing filament forms a large angle with the axis. At 5.0 kV, the meniscus assumes rim emission geometry with four cusps, each emitting a divergent jet. It seems that axial spraying modes in high conductivity systems are not formed; instead, the excess amount of charged liquid is expelled close to the axis but under an angle. It is also clear that one cannot identify Taylor cones in high conductivity systems, because conical menisci are not observed. Compared to 50% MeOH, the rim emission sets in at a significantly higher voltage producing high-frequency pulsations, and the position of the cusps in this geometry oscillates with a low frequency due to capillary waves. Further investigation of these systems is underway.

In an earlier study, we demonstrated that spraying mode changes result in altered plume distributions.[18] This, in turn, impacts the size distribution and number of charged droplets entrained into the atmospheric pressure interface of the mass spectrometer and, ultimately, the analytical signal. Thus, it is essential to maintain a particular spraying mode of ESI sources. The spray diagnostic methods described in this paper present a simple and straightforward way to detect these mode changes through monitoring the Fourier spectrum of the spray current. These diagnostic results can be used in a feedback loop to regulate spray parameters and avoid switching between spraying modes. This capability can be especially useful when liquid properties continuously change during an experiment, for example, in the combination of gradient elution HPLC with an ESI source.

We demonstrated that optimal tip designs need to minimize the possibility of contact line movements because they can be the source of spray instabilities. This might be achieved by selecting a tapered tip geometry ending in a sharp rim instead of the blunt tip used in many commercial systems as well as in this study. Another way of ensuring the stability of the contact line of the meniscus is controlling the wettability of the tip by chemical modification.

Additional practical consequences of the pulsating spray current are related to the corresponding pulsation of the ion current. In fast sampling mass spectrometers, such as the orthogonal-extraction time-of-flight systems, the sampling frequency can be comparable to the frequency of current oscillations. Although the dc component of the spray current is usually more significant, the ac current contribution may result in substantial peak intensity variations in the mass spectrum. This effect can be alleviated by synchronizing the extraction pulse to the natural pulsation of the spray. Experiments to follow the temporal variations of the ion current in an ESI system are underway in our laboratory.

ACKNOWLEDGMENT

This material is based upon work supported by the National Science Foundation under Grant No. 0415521 and by the Research Enhancement Fund of the George Washington University. The funding provided by these institutions is greatly appreciated. Any opinions, findings, and conclusions or recommendations expressed in this material are those of the authors and do not necessarily reflect the views of the National Science Foundation. Special thanks is due to Mr. I. Marginean for his help with the fast imaging experiments during this project.

Received for review March 21, 2005. Accepted April 25, 2005.

AC050475E